Published in final edited form as:

Nature. 2009 May 28; 459(7246): 596–600. doi:10.1038/nature08030.

NAADP mobilizes calcium from acidic organelles through two-pore channels

Peter J. Calcraft[1,¶], **Abdelilah Arredouani**[2,¶], **Margarida Ruas**[2,¶], **Zui Pan**[3,¶], **Xiaotong Cheng**[2,¶], **Xuemei Hao**[4,5], **Jisen Tang**[5], **Katja Rietdorf**[2], **Lydia Teboul**[6], **Kai-Ting Chuang**[2], **Peihui Lin**[3], **Rui Xiao**[5], **Chunbo Wang**[5], **Yingmin Zhu**[5], **Yakang Lin**[5], **Christopher N. Wyatt**[1], **John Parrington**[2], **Jianjie Ma**[3], **A. Mark Evans**[1], **Antony Galione**[2], and **Michael X. Zhu**[5,*]

[1]Centre for Integrative Physiology, College of Medicine and Veterinary Medicine, University of Edinburgh, Edinburgh, Scotland UK

[2]Department of Pharmacology, University of Oxford, Oxford, UK

[3]Department of Physiology and Biophysics, UMDNJ-Robert Wood Johnson Medical School, Piscataway, NJ, USA

[4]College of Life Sciences, Peking University, Beijing, China

[5]Department of Neuroscience and Center for Molecular Neurobiology, The Ohio State University, Columbus, OH, USA

[6]MRC Harwell, Oxfordshire, UK

Abstract

Ca^{2+} mobilization from intracellular stores represents an important cell signaling process 1 which is regulated, in mammalian cells, by inositol 1,4,5-trisphosphate ($InsP_3$), cyclic ADP ribose (cADPR) and nicotinic acid adenine dinucleotide phosphate (NAADP). $InsP_3$ and cADPR release Ca^{2+} from sarco / endoplasmic reticulum (S/ER) stores through activation of $InsP_3$ and ryanodine receptors ($InsP_3$Rs and RyRs). By contrast, the nature of the intracellular stores targeted by NAADP and molecular identity of the NAADP receptors remain controversial 1,2, although evidence indicates that NAADP mobilizes Ca^{2+} from lysosome-related acidic compartments 3,4. Here we show that two-pore channels (TPCs) comprise a family of NAADP receptors, with TPC1 and TPC3 being expressed on endosomal and TPC2 on lysosomal membranes. Membranes enriched with TPC2 exhibit high affinity NAADP binding and TPC2 underpins NAADP-induced Ca^{2+} release from lysosome-related stores that is subsequently amplified by Ca^{2+}-induced Ca^{2+} release via $InsP_3$Rs. Responses to NAADP were abolished by disrupting the lysosomal proton gradient and by ablating TPC2 expression, but only attenuated by depleting ER Ca^{2+} stores or blocking $InsP_3$Rs. Thus, TPCs form NAADP receptors that release Ca^{2+} from acidic organelles, which can trigger additional Ca^{2+} signals via S/ER. TPCs therefore provide new insights into the

[*]Address correspondence to: Dr. Michael X. Zhu, Center for Molecular Neurobiology, The Ohio State University, 168 Rightmire Hall, 1060 Carmack Road, Columbus, OH 43210, USA. Tel: (614)292-8173, Fax: (614)292-5379, email: zhu.55@osu.edu.

[¶]Equal contributing authors

The authors declare no competing financial interests.

regulation and organization of Ca^{2+} signals in animal cells and will advance our understanding of the physiological role of NAADP.

NAADP was first identified as a potent intracellular Ca^{2+} mobilizing agent in sea urchin eggs 5 and later confirmed as such in various mammalian preparations 6-8. The Ca^{2+} stores mobilized by NAADP appear to be distinct from S/ER 9-11 and accumulating evidence from a variety of preparations now suggests that NAADP targets lysosome-like acidic compartments 3,4,12-14. However, it remains debated whether NAADP can also release the S/ER Ca^{2+} stores in certain cell types, perhaps by directly acting on RyRs 15-17. Furthermore, cross-talk between NAADP signaling and that mediated by $InsP_3$, Ca^{2+}, and cADPR exists in many cell types 11,18 (Supplementary Fig. S1), complicating the interpretation of experimental results.

TPCs (also known as *TPCN*s) are novel members of the superfamily of voltage-gated ion channels 19,20. Their predicted structures indicate 2-fold symmetry with a total of 12 putative transmembrane (TM) α-helices (Fig. 1a). Three non-allelic *TPCN* genes are present in sea urchins and most vertebrate species, with TPC3 absent in primates and some rodent species (supplementary Fig. S2). The three TPCs are equally distant from each other, and from plant "TPC1", with <30% amino acid identity in the conserved TM regions (Fig. 1b and supplementary Fig. S2). While *Arabidopsis* "TPC1" has been shown to mediate Ca^{2+} release from plant intracellular vacuoles 21, functional data are lacking for animal TPCs.

Similar to the reported widespread expression of TPC1 mRNA 19, Northern analysis shows that human TPC2 (hTPC2) mRNA is expressed in most human tissues with higher levels in liver and kidney (Fig. 1c). Immunofluorescence labeling of HEK293 cells using an anti-hTPC2 antibody (see supplementary Fig. S3) revealed punctate staining in the cytoplasm, which was blocked by the antigenic peptides (not shown) and overlaps with that of lysosome-membrane associated protein 2 (LAMP-2; Fig. 1d, Pearson's coefficient = 0.92). Similarly, in a stable cell line expressing hemagglutinin (HA) tagged-hTPC2 (hTPC2 cells), the HA-tagged protein colocalizes with LAMP-2 (Fig. 1e; Supplementary Movie 1, Table, and Fig. S4) but not with markers for early and late endosomes or that for ER, Golgi, or mitochondria (Supplementary Figs. S5a-e). Moreover, LysoTracker (Fig. 1f), but not MitoTracker or fluorescent transferrin (not shown), accumulated in intracellular vesicles surrounded by HA-hTPC2. Similar results were obtained for heterologously expressed mouse TPC2 (Supplementary Fig. S6).

In contrast, heterologously expressed TPC1 and TPC3 display only sparse co-localization with TPC2 or LAMP-2, but instead are predominantly expressed in endosomes and other unidentified intracellular compartments (Supplementary Figs. S5f, S5g, S7, and Table). Therefore, all mammalian TPCs are expressed intracellularly on endo-lysosomes with TPC2 being specifically targeted to lysosomal membranes.

The lysosomal localization and homology to Ca^{2+} channels prompted us to test whether TPC2 forms a binding site for NAADP. Membranes from the hTPC2 and wild type HEK293 cells were incubated with 0.2 nM [^{32}P]NAADP in the absence and presence of unlabeled NAADP (100 μM). hTPC2 membranes showed more than a three-fold increase in specific

binding compared to wild type membranes (Fig. 2a). To confirm that the binding is associated with expressed TPC2 proteins, we depleted HA-hTPC2 from the membranes with an anti-HA antibody and tested [^{32}P]NAADP binding to the resulting supernatant and pellet. With anti-HA the binding was mainly associated with the pellet whereas with a control antibody it remained in the supernatant (Fig. 2b).

A ligand competition assay showed that the hTPC2-containing membranes displayed two affinities to NAADP with K_d values of 5.0 ± 4.2 nM and 7.2 ± 0.8 μM (n = 3) (Fig. 2c). This binding curve closely resembles that of mouse liver membranes (Fig. 2d), which displayed affinity values of 6.6 ± 3.5 nM and 4.6 ± 2.4 μM (n = 4), and these K_d for the high affinity binding site compare well with results reported for other mammalian preparations 22-24.

As expected 22,25, NADP, the precursor of NAADP that is unable to mobilize Ca^{2+}, only showed low affinity binding to hTPC2 and mouse liver membranes, with K_d of 10.3 ± 3.1 μM (n = 3) and 4.5 ± 2.3 μM (n = 4), respectively. This could also arise from contamination by trace amounts of NAADP in NADP preparations 5. Moreover, although wild type membranes displayed specific binding to NAADP, the ligand competition assay could only reveal low affinity binding, indicating that the fraction for high affinity binding must be very low. This is supported by quantitative RT-PCR which showed a >250 fold increase in TPC2 mRNA in hTPC2 compared to wild type cells (Supplementary information). Therefore, TPC2 expression confers the high affinity NAADP binding. Although we cannot exclude that interactions with accessory proteins may be necessary for NAADP binding to TPC2, such proteins would have to associate with TPC2 tightly in order to explain these binding results.

To test if TPC2 mediates Ca^{2+} release from lysosomes, we studied the effect of flash photolysis of caged-NAADP on intracellular Ca^{2+} concentration ($[Ca^{2+}]_i$) in wild type HEK293 and hTPC2 cells by Fluo3 fluorescence. As shown in Fig. 3a*i*, all hTPC2 cells responded to photorelease of NAADP with a biphasic $[Ca^{2+}]_i$ transient comprising an initial slow pacemaker-like ramp (10-180 sec) and a subsequent large Ca^{2+} transient. No fluorescence increase occurred after UV flashes if caged-NAADP was not included (n=6, not shown). Furthermore, wild type cells displayed only small and short-lived $[Ca^{2+}]_i$ rises and lacked both the ramp-like phase and the secondary transient (Fig. 3b).

Consistent with a role for lysosomes in this process, the vacuolar H^+-ATPase inhibitor bafilomycin A1 (Baf, 1 μM) abolished both phases of the response to NAADP (Fig. 3a*iv*), but failed to affect the $[Ca^{2+}]_i$ rise induced by extracellular application of 100 μM ATP, which activates ER Ca^{2+} release (not shown). By contrast, inclusion of heparin (200 μg/ml), a competitive inhibitor of $InsP_3Rs$, in the patch pipette only blocked the secondary phase of the Ca^{2+} transient and thereby revealed in its entirety the initial $[Ca^{2+}]_i$ signal triggered by NAADP (Fig. 3a*ii*). Consistent with the lack of RyR expression in HEK293 cells 26, both phases of the response to photorelease of NAADP persisted in hTPC2 cells preincubated with 10 μM ryanodine (not shown). Furthermore, the combined effects of depleting the ER store by pretreatment with thapsigargin (TG, 1 μM), blocking $InsP_3Rs$ with heparin and RyRs with ryanodine caused no further inhibition of the NAADP-induced response than did blocking $InsP_3Rs$ with heparin alone (Fig. 3a*iii* and 3c). Therefore, the initial $[Ca^{2+}]_i$ rise is

dependent on acidic organelles but independent of the ER, whereas the secondary phase is due to ER Ca^{2+} release via $InsP_3Rs$, presumably through Ca^{2+}-induced Ca^{2+} release in concert with resting $InsP_3$ levels.

To determine the concentration-response relationship for NAADP, we dialyzed known concentrations of NAADP into single cells via patch pipettes and monitored $[Ca^{2+}]_i$ changes using Fura2 13,18. In hTPC2 cells, while 100 pM NAADP did not cause any appreciable $[Ca^{2+}]_i$ rise, 10 nM NAADP elicited a biphasic response reminiscent of those evoked by photolysis of caged-NAADP (Fig. 3d*i* and 3d*ii*). Pretreatment with TG abolished the second but not the first phase (Fig. 3d*iii*). The response was also seen with 1 μM but not with much higher NAADP concentrations (1 mM, Fig. 3f), consistent with the notion that NAADP-induced Ca^{2+} release desensitizes at high ligand concentrations 6. By contrast, 10 nM NAADP was without effect in wild type cells, while 1 μM only induced a small, perhaps more localized, Ca^{2+} transient in 3 out of 5 cells (Figs. 3e and 3f).

Again, the Ca^{2+} transient induced by intracellular dialysis of 10 nM NAADP in hTPC2 cells was blocked by Baf. More importantly, the response was abolished by transfection into hTPC2 cells of an shRNA against TPC2 (Supplementary Fig. S8), but not that of a scrambled control shRNA (Fig. 3f), demonstrating the essential role of TPC2 in mediating NAADP-induced Ca^{2+} release. All cells responded to extracellularly applied carbachol, which triggers ER Ca^{2+} release, indicating that cells were viable 27.

To examine the role of endogenous TPC2 in NAADP signaling in a native system, we generated TPC2 knockout mice using a gene trap strategy (Figs. 4a-c and supplementary information) 29 and isolated pancreatic β cells in which previous studies have established that NAADP-dependent Ca^{2+} mobilization from a TG-insensitive acidic store 12,24 underpins the gating of a Ca^{2+}-activated plasma membrane cation current. Fig. 4d shows that under the whole-cell configuration, intracellular dialysis of 100 nM NAADP elicited oscillatory inward currents in wild type β-cells held at -70 mV. No such currents were detected if NAADP was omitted from the pipette solution, if intracellular Ca^{2+} was strongly buffered by 10 mM BAPTA, or if the extracellular cations were replaced by N-methyl-D-glucamine (not shown). Strikingly, NAADP failed to activate the cation currents in β-cells from the TPC2 knockout mice (Fig. 4e), strongly suggesting that TPC2 plays a critical role in native NAADP-evoked Ca^{2+} signaling in β-cells.

The above results are best explained if TPC2 is a lysosomal Ca^{2+} release channel targeted by NAADP. Although we have focused on TPC2 because of its predominant lysosomal localization, TPC1 and TPC3 may also mediate NAADP-induced Ca^{2+} release from distinct subsets of acidic organelles, such as the distinguished endosome populations suggested by their subcellular distributions. Indeed, we have observed significant but highly localized Ca^{2+} transients in response to 10 nM NAADP in cells that overexpress human TPC1 as opposed to the global $[Ca^{2+}]_i$ changes seen in hTPC2 cells (Supplementary Fig. S9 and Movie 2). This distinction is consistent with the more restricted subcellular distribution of TPC1 compared to TPC2 (Supplementary Fig. S7).

The biphasic Ca^{2+} response to NAADP in hTPC2 overexpressing cells and the dependence of the later phase on $InsP_3Rs$ and the ER are consistent with the idea that NAADP-induced Ca^{2+} signals are small, and perhaps localized, but able to act, at least via TPC2, as discrete triggers for large global $[Ca^{2+}]_i$ changes through coupling to $InsP_3R$/RyR-S/ER systems. This adds an intriguing possibility for signal diversification, given that the pure NAADP-evoked Ca^{2+} signal is small and highly localized once the ER Ca^{2+} store is depleted by TG, as shown in Figs 3a*iii* and 3d*iii* for heterologously expressed TPC2 as well as the endogenous channels in human hepatoblastoma cell line, HepG2 (Supplementary Fig. S10). However, the localized Ca^{2+} signals will likely reach high levels, particularly at lysosome-ER junctions with unheralded versatility supplied by the fact that TPC-containing vesicles undergo rapid movement within the cytosoplasm (Supplementary Movie 3). In this respect it is important to note that NAADP-sensitive Ca^{2+} signals can have multiple coupling targets. In sea urchin eggs and pancreatic acinar cells, NAADP-induced Ca^{2+} signals are coupled to ER Ca^{2+} release through $InsP_3Rs$ and RyRs 6,11,28; in pulmonary arterial smooth muscle cells, they appear to selectively target RyRs 13,18; in pancreatic β-cells, they are coupled to Ca^{2+}-activated cation channels. Thus, the graded local and mobile endo-lysosome-derived Ca^{2+} signals released via TPCs, through coupling to other systems, are dynamic and versatile. Future investigations on the role of TPCs as NAADP receptors will therefore provide important advances in our understanding of the mechanisms of regulation, spatial organization and diverse functional roles of Ca^{2+} signals in mammalian cells.

Method summary

The cDNA for hTPC2 was cloned from HEK293 cells by RACE-PCR. Northern hybridization was performed using a multi-tissue human mRNA blot (BD Biosciences). For stable expression, the N-terminal HA-tagged hTPC2 was placed in pIRESneo (BD Biosciences), transfected in HEK293 cells, and stable clones selected and maintained using G418. [^{32}P]NAADP synthesis, membrane purification and radioligand binding studies were carried out as previously described 23,25. Caged-NAADP was synthesized as described 30. TPC2 knockout mice were developed from an ES cell line (YHD437) containing a gene trap mutation in the *Tpcn2* gene. Details for flash photolysis of caged-NAADP, intracellular NAADP dialysis, Ca^{2+} imaging, and measurement of Ca^{2+}-activated cation currents are described in additional methods.

Supplementary Material

Refer to Web version on PubMed Central for supplementary material.

Acknowledgements

This work was supported by grants from the UK Wellcome Trust and the British Heart Foundation to AG, JP and AME, the US National Institutes of Health to MXZ and JM, and the American Heart Association to MXZ. AG was a Wellcome Senior Research Fellow in basic Biomedical Science. The work of AME was funded by a Wellcome Trust Project Grant (CNW, reference number 070772) and a British Heart Foundation Studentship (PJC, reference number FS/05/050). We thank Drs. T. Kong and W. Li of Rutgers University for the HepG2 cell line, O. Ogunbayo of University of Edinburgh for technical assistance, and F. Platt and A. Morgan of University of Oxford and M. Viapiano of Ohio State University for help with the manuscript.

The following sequences have been deposited in the GenBank database: AY029200 (hTPC2), AY083666 (hTPC1), EU344154 (chicken TPC3), EU344155 (rabbit TPC3), BK006366 (dog TPC3), BK006367 (Zebrafish TPC3), BK006368 (horse TPC3), BK006573 (bovine TPC3).

Additional methods

Sequence analysis

For sequence alignment (Fig. 1b), the second TM domain of TPCs and the fourth TM domain of Ca_v and Na_v were aligned with the TM domains (including all six TM segments and the pore-loop) of selected TRP members and CatSpers. GenBank accession numbers are given in supplementary Fig. S2. The phylogenetic tree was generated by ClustalW (http://align.genome.jp) and plotted using a Neighbour-Joining algorithm.

DNA constructs and stable cell lines

The cDNA for hTPC2 was cloned from HEK293 cells by RACE-PCR using primers designed against the expressed sequence tag AA309878. Northern hybridization was performed using a multi-tissue human mRNA blot (BD Biosciences) and random-labeled cDNA probes against a BglII fragment (nucleotides 1547-2012) of hTPC2 mRNA. The cDNA for hTPC1 was obtained from Research Genetics (Clone ID: CS0DB002YA14) and confirmed by DNA sequencing. For stable expression, the HA epitope was added to the N-terminus of hTPC2 and the cDNA placed in the pIRESneo vector (BD Biosciences). A His_6-tag was added to the C-terminus of hTPC1 and the cDNA placed in the pIREShyg2 vector (BD Biosciences). Transfection into HEK293 cells was performed using Lipofectamine 2000 (Invitrogen) following the manufacturer's protocol. Stable clones were selected and maintained in regular culture medium containing 400 μg/ml G418 (for hTPC2) or 100 μg/ml hygromycin B (for hTPC1). Monoclonal cell lines were established through limiting dilution.

Immunocytochemistry

A polyclonal anti-hTPC2 antibody was made by immunizing rabbits with two synthetic peptides (GGKQDDGQDRERLTY and VKEHPPRPEYQSPFL) conjugated to keyhole limpet hemocyanin and affinity purified using the antigenic peptides. Cells were seeded onto poly-ornithine coated coverslips and grown overnight. After washing in phosphate-buffered saline (PBS, pH 7.4), the cells were fixed using ice-cold methanol (-20 °C, 15 min, Fig. 1d) or 4% paraformaldehyde (22 °C, 1 hr, Fig. 1e) and blocked using 5% dry milk in PBS. Immunostaining followed standard protocols. The rabbit anti-hTPC2 antibody was diluted 1:200 and the secondary antibody (1:500) was an Alexa 488-conjugated anti-rabbit IgG (Invitrogen). The rat anti-HA antibody (Roche) was diluted 1:500. The secondary antibody (1:500) was an Alexa 488-conjugated anti-rat IgG (Invitrogen). Mouse anti-LAMP-2 monoclonal antibody (Developmental Studies Hybridoma Bank) was diluted 1:500. The secondary anti-mouse antibodies (1:500) were conjugated with Alexa 594. Incubations were at 4 °C overnight. All washes were carried out in the dark at room temperature using PBS containing 0.05% tween 20. The washed slides were mounted using Gel/MountTM (BioMeda). Images were acquired using a Leica TCS SL laser scanning confocal system on

a Leica DMIRE2 inverted microscope with a 100x 1.4 n.a. oil immersion objective and a pinhole of 182 μm. DIC images were acquired simultaneously to show the shape of corresponding cells.

LysoTracker labeling and imaging

hTPC2 cells were incubated with 200 ng/ml LysoTracker Red DND-99 (Invitrogen) for 30 min and then fixed with 4% paraformaldehyde and immunostaining using the rat anti-HA antibody as described above. Images were taken using a Bio-Rad MRC 1000 confocal system attached to a Nikon Optiphoto-2 microscope equipped with a 60x 1.4 n.a. oil immersion objective, at iris 2.0 and a z step size at 0.5 μm.

NAADP-binding experiments

[^{32}P]NAADP synthesis, membrane purification and radioligand binding studies were carried out as previously described 23,25. Briefly, membranes were incubated with 0.2 nM [^{32}P]NAADP together with or without 100 μM unlabelled NAADP at room temperature for 60 min and terminated by rapid vacuum filtration through GF/B filters. For ligand competition assays, membranes were pre-incubated with desired concentrations of unlabeled NAADP or NADP at room temperature for 10 min before 0.2 nM [^{32}P]NAADP was added and the incubation continued for another 60 min. Immunodepletion experiments were performed by immunoprecipitation (IP) of microsomal membranes of hTPC2 cells solubilized for 60 min at 4 °C in IP buffer containing (mM) 150 NaCl, 20 HEPES, 1 EDTA (pH 7.2) with 1% CHAPS and 1× proteinase inhibitor. The same amount of solubilized membrane was incubated with the indicated antibodies at 4 °C overnight and then bound to Protein G sepharose beads (GE Healthcare, 120 min, 4 °C). Beads were centrifuged at 1,000 × g for 1 min and supernatants collected. Beads were washed 3 times with IP buffer and bound proteins were either eluted with Laemmli buffer for western blotting or used for [^{32}P]NAADP binding. For solubilized IP samples, extracts (same amount of total protein) were incubated in Glu-IM (in mM: 250 potassium gluconate, 250 N-methylglucamine, 20 HEPES, 1 MgCl, pH 7.2) supplemented with 0.2 nM [^{32}P]NAADP with or without 10 μM of unlabelled NAADP for 60 min at 22°C. Then 500 μg γ-globulin (Sigma) and polyethylene glycol (15%, w/v, Sigma) were added and the incubation continued for 30 min. After centrifugation at 13,000 × g for 5 min, the pellets were washed with 15% (w/v) polyethylene glycol and dissolved in H_2O for scintillation counting. For proteins coupled to agarose beads, the beads were incubated with Glu-IM as described above and then washed 3 times with Glu-IM. Proteins were eluted by the addition of 2% SDS, collected and spotted on GF/B filters for determining radioactivity by phosphorimaging.

Flash photolysis of caged-NAADP and measurement of $[Ca^{2+}]_i$ changes

Wild type HEK293 and hTPC2 cells were seeded at low density (10% confluency) onto poly-D-lysine coated tissue culture dishes (FluoroDish; World Precision Instruments) one day before the experiments. The intracellular solution contained (mM): 140 KCl, 1 $MgCl_2$, 10 Hepes and 0.1 Fluo3 pentapotassium (pH 7.2 with KOH). The bath was a physiological salt solution (PSS) that contained (mM): 130 NaCl, 5.2 KCl, 1$MgCl_2$, 1.7 $CaCl_2$, 10

glucose, 10 Hepes (pH 7.4 with NaOH). Cells were held at -40 mV in the whole-cell configuration with the pipette solution containing 10 μM caged-NAADP. When needed, heparin (200 μg/ml) was added to the intracellular solution; TG (1 μM), ryanodine (10 μM), and Baf (1 μM) were included in the bath for preincubation. Fluo3 was excited at 490 nm and fluorescence emission at 530 nm was monitored using a photomultiplier tube. The caged-NAADP was photolysed with an XF-10 arc lamp (HI-TECH Scientific). To avoid prolonged UV exposure, multiple 10-ms UV flashes, shown as downward strokes in Figs. 3a and 3b, were applied to yield sufficient photolysis of caged-NAADP, which has a much lower uncaging efficiency than most other caged compounds, e.g. caged-$InsP_3$. 10 μM caged-NAADP was found to be optimal because higher concentrations yielded no response, presumably due to desensitization caused by the presence of trace amounts of free NAADP in the caged preparation and/or the bell-shaped dose response relation to NAADP 6.

Intracellular dialysis of NAADP and Ca^{2+} imaging

NAADP was applied intracellularly in the whole-cell configuration of the patch-clamp technique, adapted from an established protocol described previously 13. Briefly, cells grown on poly-D-lysine coated glass-bottom dishes overnight were incubated for 30 min with Fura2 AM (5 μM) in PSS. Dishes were placed on a Leica DMIRBE inverted microscope and superfused with Fura2 free PSS for at least 30 min prior to experimentation. Control and NAADP pipette solutions containing (mM): 140 KCl, 10 Hepes, 1 $MgCl_2$ and 5 μM Fura2, pH 7.4 and the desired concentration of NAADP, were applied by intracellular dialysis from a patch pipette while the cell was held at -40 mV in the whole-cell configuration. Intracellular Ca^{2+} concentration was reported by Fura2 fluorescence ratio (F340/F380 excitation; emission 510 nm). Emitted fluorescence was recorded at 22 °C with a sampling frequency of 0.2 Hz, using a Hamamatsu 4880 CCD camera via a Zeiss Fluar 40x, 1.3 n.a. oil immersion lens and Leica DMIRBE microscope. The seal resistance, as measured using an Axopatch 200B amplifier (Axon instruments), was ≥ 2 GΩ throughout each experiment. Series resistance and pipette resistance were ≤ 10 MΩ and ≤ 3 MΩ, respectively. Background subtraction was performed on-line. Analysis was via Openlab imaging software (Improvision). When needed, the hTPC2 cells were preincubated with TG (1 μM) for 30 min or Baf (100 nM) for 45 min. Method for shRNA transfection is described in supplementary information.

Measurement of NAADP-sensitive cation currents in pancreatic β cells

Islets of Langerhans were obtained by collagenase digestion of the pancreas, and single cells were prepared by dispersion of islet cells in a Ca^{2+}-free medium. Cells were cultured for 1-4 days in RPMI 1640 medium containing 10 mM glucose.

NAADP was infused through a patch pipette in the whole-cell configuration. The pipette solution contained (mM): 125 K^+-glutamate, 10 KCl, 10 NaCl, 10 KCl, 1 $MgCl_2$, 3 Mg-ATP, 0.1 Na-GTP, 10 EGTA and 5 Hepes (pH 7.2 with KOH). NAADP was added at a final concentration of 100 nM. The bath solution contained (mM): 120 NaCl, 4.8 KCl, 2.5 $CaCl_2$, 1.2 $MgCl_2$, 24 $NaHCO_3$, 10 glucose, 5 Hepes (pH 7.4 with NaOH). The holding potential was -70 mV. The experiments were carried out at room temperature using Multiclamp 700B

and the software pClamp 9 (Axon Instruments). Patch pipettes were pulled from borosilicate glass capillaries (World Precision Instruments) to give a resistance of 3-5 MΩ when filled with the pipette solution.

References

1. Berridge MJ, Bootman MD, Roderick HL. Calcium: Calcium signalling: dynamics, homeostasis and remodelling. Nat. Rev. Mol. Cell Biol. 2003; 4:517–529. [PubMed: 12838335]
2. Galione A, Churchill GC. Interactions between calcium release pathways: multiple messengers and multiple stores. Cell Calcium. 2002; 32:343–354. [PubMed: 12543094]
3. Churchill GC, et al. NAADP mobilizes Ca^{2+} from reserve granules, a lysosome-related organelle, in sea urchin eggs. Cell. 2002; 111:703–708. [PubMed: 12464181]
4. Yamasaki M, et al. Organelle selection determines agonist-specific Ca^{2+} signals in pancreatic acinar and beta cells. J. Biol. Chem. 2004; 279:7234–7240. [PubMed: 14660554]
5. Lee HC, Aarhus R. A derivative of NADP mobilizes calcium stores insensitive to inositol trisphosphate and cyclic ADP-ribose. J. Biol. Chem. 1995; 270:2152–2157. [PubMed: 7836444]
6. Cancela JM, Churchill GC, Galione A. Coordination of agonist-induced Ca^{2+}-signalling patterns by NAADP in pancreatic acinar cells. Nature. 1999; 398:74–76. [PubMed: 10078532]
7. Bak J, et al. Nicotinic acid adenine dinucleotide phosphate triggers Ca^{2+} release from brain microsomes. Curr. Biol. 1999; 9:751–754. [PubMed: 10421579]
8. Berg I, Potter BV, Mayr GW, Guse AH. Nicotinic acid adenine dinucleotide phosphate ($NAADP^{+}$) is an essential regulator of T-lymphocyte Ca^{2+}-signaling. J. Cell Biol. 2000; 150:581–588. [PubMed: 10931869]
9. Genazzani AA, Galione A. Nicotinic acid-adenine dinucleotide phosphate mobilizes Ca^{2+} from a thapsigargin-insensitive pool. Biochem. J. 1996; 315:721–725. [PubMed: 8645149]
10. Lee HC, Aarhus R. Functional visualization of the separate but interacting calcium stores sensitive to NAADP and cyclic ADP-ribose. J. Cell Sci. 2000; 113:4413–4420. [PubMed: 11082034]
11. Churchill GC, Galione A. NAADP induces Ca^{2+} oscillations via a two-pool mechanism by priming IP_3- and cADPR-sensitive Ca^{2+} stores. EMBO J. 2001; 20:2666–2671. [PubMed: 11387201]
12. Mitchell KJ, Lai FA, Rutter GA. Ryanodine receptor type I and nicotinic acid adenine dinucleotide phosphate receptors mediate Ca^{2+} release from insulin-containing vesicles in living pancreatic beta-cells (MIN6). J. Biol. Chem. 2003; 278:11057–11064. [PubMed: 12538591]
13. Kinnear NP, Boittin FX, Thomas JM, Galione A, Evans AM. Lysosome-sarcoplasmic reticulum junctions. A trigger zone for calcium signaling by nicotinic acid adenine dinucleotide phosphate and endothelin-1. J. Biol. Chem. 2004; 279:54319–54326. [PubMed: 15331591]
14. Macgregor A, et al. NAADP controls cross-talk between distinct Ca^{2+} stores in the heart. J. Biol. Chem. 2007; 282:15302–15311. [PubMed: 17387177]
15. Mojzisová A, Krizanová O, Záciková L, Komínková V, Ondrias K. Effect of nicotinic acid adenine dinucleotide phosphate on ryanodine calcium release channel in heart. Pflugers Arch. 2001; 441:674–677. [PubMed: 11294249]
16. Gerasimenko JV, et al. NAADP mobilizes Ca^{2+} from a thapsigargin-sensitive store in the nuclear envelope by activating ryanodine receptors. J. Cell Biol. 2003; 163:271–282. [PubMed: 14568993]
17. Dammermann W, Guse AH. Functional ryanodine receptor expression is required for NAADP-mediated local Ca^{2+} signaling in T-lymphocytes. J. Biol. Chem. 2005; 280:21394–21399. [PubMed: 15774471]
18. Boittin FX, Galione A, Evans AM. Nicotinic acid adenine dinucleotide phosphate mediates Ca^{2+} signals and contraction in arterial smooth muscle via a two-pool mechanism. Circ. Res. 2002; 91:1168–1175. [PubMed: 12480818]
19. Ishibashi K, Suzuki M, Imai M. Molecular cloning of a novel form (two-repeat) protein related to voltage-gated sodium and calcium channels. Biochem. Biophys. Res. Commun. 2000; 270:370–376. [PubMed: 10753632]

20. Anderson PA, Greenberg RM. Phylogeny of ion channels: clues to structure and function. Comp. *Biochem. Physiol. B. Biochem. Mol. Biol.*. 2001; 129:17–28. [PubMed: 11337248]
21. Peiter E, et al. The vacuolar Ca^{2+}-activated channel TPC1 regulates germination and stomatal movement. Nature. 2005; 434:404–408. [PubMed: 15772667]
22. Bak J, Billington RA, Timar G, Dutton AC, Genazzani AA. NAADP receptors are present and functional in the heart. Curr. Biol. 2001; 11:987–990. [PubMed: 11448777]
23. Patel S, Churchill GC, Sharp T, Galione A. Widespread distribution of binding sites for the novel Ca^{2+}-mobilizing messenger, nicotinic acid adenine dinucleotide phosphate, in the brain. J. Biol. Chem. 2000; 275:36495–36497. [PubMed: 11010959]
24. Masgrau R, Churchill GC, Morgan AJ, Ashcroft SJ, Galione A. NAADP: a new second messenger for glucose-induced Ca^{2+} responses in clonal pancreatic beta cells. Curr. Biol. 2003; 13:247–251. [PubMed: 12573222]
25. Patel S, Churchill GC, Galione A. Unique kinetics of nicotinic acid-adenine dinucleotide phosphate (NAADP) binding enhance the sensitivity of NAADP receptors for their ligand. Biochem. J. 2000; 352:725–729. [PubMed: 11104679]
26. Aoyama M, et al. Requirement of ryanodine receptors for pacemaker Ca^{2+} activity in ICC and HEK293 cells. J. Cell Sci. 2004; 117:2813–2825. [PubMed: 15169838]
27. van Koppen CJ, Meyer zu Heringdorf D, Alemany R, Jakobs KH. Sphingosine kinase-mediated calcium signaling by muscarinic acetylcholine receptors. Life Sci. 2001; 68:2535–2540. [PubMed: 11392623]
28. Cancela JM, Gerasimenko OV, Gerasimenko JV, Tepikin AV, Petersen OH. Two different but converging messenger pathways to intracellular Ca^{2+} release: the roles of nicotinic acid adenine dinucleotide phosphate, cyclic ADP-ribose and inositol trisphosphate. EMBO J. 2000; 19:2549–2557. [PubMed: 10835353]
29. Stryke D, et al. BayGenomics: a resource of insertional mutations in mouse embryonic stem cells. Nucleic Acids Res. 2003; 31:278–281. [PubMed: 12520002]
30. Morgan, AJ., et al. Methods in cyclic ADP-Ribose and NAADP research. In: Putney, JW., Jr., editor. Methods in Calcium Signalling. 2nd edition. CRC Press; Boca Raton: 2006. p. 267-334.

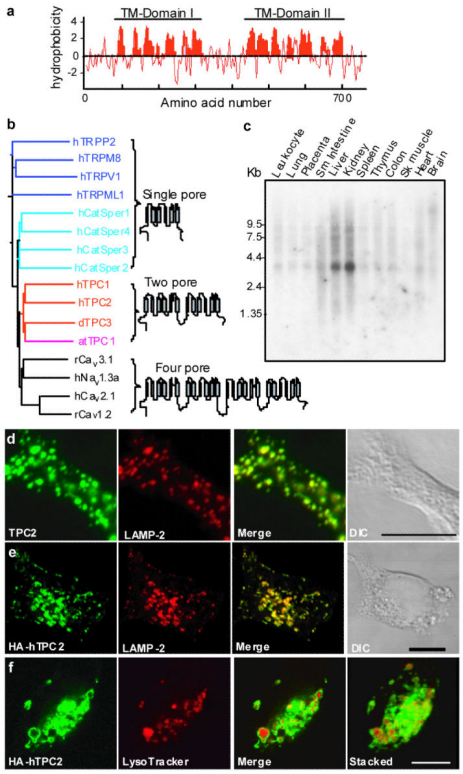

Figure 1. Tissue and subcellular expression of mammalian TPC2

a, Hydropathy plot of human TPC2. Window size = 9 a.a. **b**, Evolutionary relationships of TPCs with single-pore and four-pore domain channels. h, human; d, dog; r, rat; at, *Arabidopsis thaliana*. **c**, Northern blot analysis of TPC2 expression in human tissues. **d**, Colocalization of endogenous TPC2 with LAMP-2 in untransfected HEK293 cells. **e** and **f**, Colocalization of HA-hTPC2 with LAMP-2 (**e**) and LysoTracker (**f**) in hTPC2 stable cell line. Right panel in **f** shows stacked image of overall LysoTracker accumulation relative to expressed HA-hTPC2 (3D projections, supplementary Movie 1). Scale bars = 10 μm.

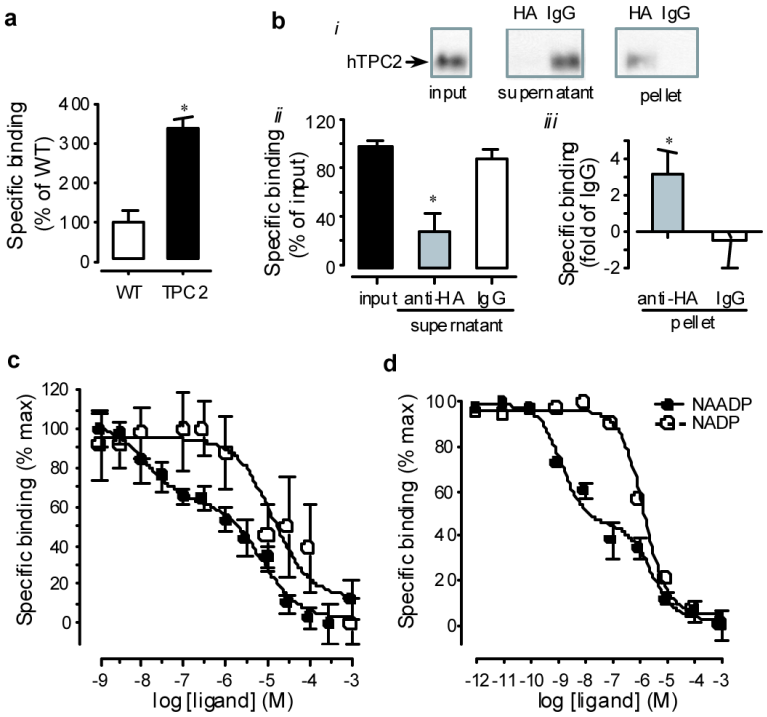

Figure 2. [^{32}P]NAADP binding to TPC2

a, Specific binding for membranes from wild type HEK293 and hTPC2 cells (n = 3). **b**, Depletion of hTPC2 by immunoprecipitation abolished [^{32}P]NAADP binding. The supernatant was depleted of hTPC2 (*i*) and [^{32}P]NAADP binding (*ii*) by anti-HA but not by rat IgG (control) antibody; hTPC2 (*i*) and [^{32}P]NAADP binding (*iii*) appeared in the pellet with anti-HA only. **c** and **d**, Representative ligand competition assay for membranes prepared from hTPC2 cells (**c**) and mouse liver (**d**). The maximal specific binding for hTPC2 membranes ranged from 167.6 to 300 dpm and for mouse liver from 1,000 to 1,600 dpm.

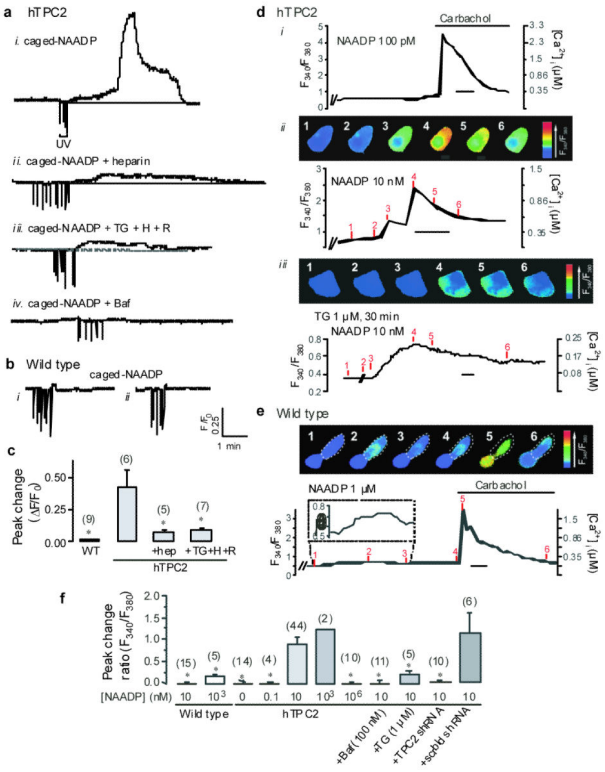

Figure 3. TPC2 expression and NAADP-evoked Ca^{2+} signaling

a-c, Effect of photoreleased NAADP on Fluo3 fluorescence in hTPC2 (**a**) and wild type HEK293 cells (**b**). **c**, Means ± SEM of peak response. H: heparin, R: ryanodine. * $p < 0.05$ different from hTPC2 only. **d-f**, Effect of intracellular dialysis of NAADP on Fura2 ratio in hTPC2 (**d**) and wild type (**e**, the cell within dashed lines) cells: upper panels pseudocolour images, lower panels ratio against time. Time scale bars = 20 s. **f**, Means ± SEM (except n = 2) of peak response. * $p < 0.05$ different from hTPC2, 10 nM NAADP. Baf: bafilomycin, scrbld: scrambled. Number of cells in parentheses.

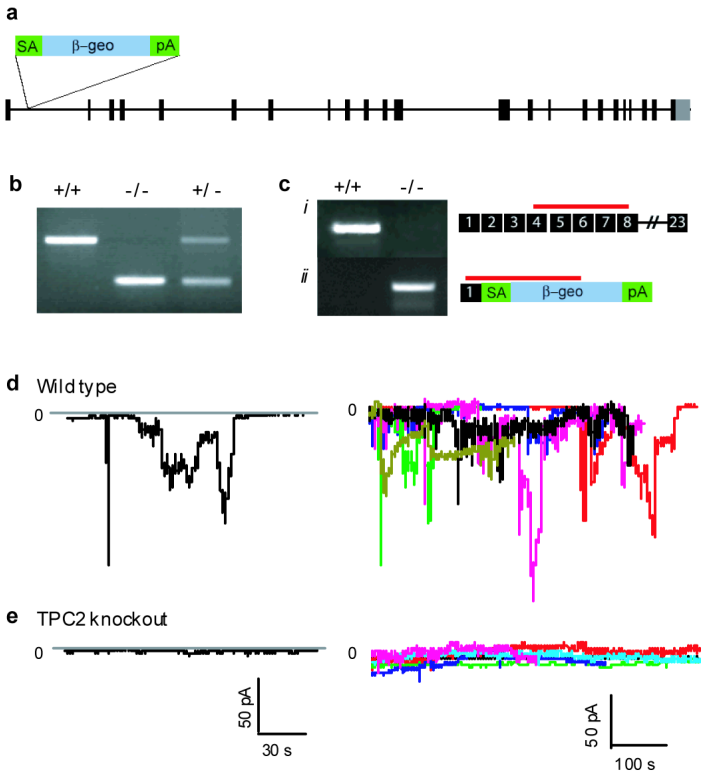

Figure 4. Pancreatic β cells from TPC2 knockout mice are NAADP insensitive

a, Approximate position of the gene trap vector in *Tpcn*2 gene. **b**, PCR analysis of genomic DNA. +/+, wild type; +/-, heterozygote; -/-, homozygote. **c**, RT-PCR products from wild type and mutant *Tpcn*2 mRNAs with approximate positions of amplicons indicated by red bars; numbers indicate exons (see supplementary information for details). **d** and **e**, Cation currents at -70 mV evoked by intracellular dialysis of 100 nM NAADP in pancreatic β-cells isolated from wild type (**d**) and TPC2 knockout (**e**) mice. *Left*, representative traces from single cells; *right*, overlaid traces for 5 cells.